Inorganic Chemistry

Article

pubs.acs.org/IC

Insertion of Trivalent Lanthanides into Uranyl Vanadate Layers and Frameworks

Yaxing Wang,[†,‡] Xuemiao Yin,[†,‡] Yanyan Zhao,[†,‡] Yang Gao,[†,‡] Lanhua Chen,[†,‡] Zhiyong Liu,[†,‡] Daopeng Sheng,[†,‡] Juan Diwu,[†,‡] Zhifang Chai,[†,‡] Thomas E. Albrecht-Schmitt,[§] and Shuao Wang*[,†,‡]

[†]School for Radiological and Interdisciplinary Sciences (RAD-X) and [‡]Collaborative Innovation Center of Radiation Medicine of Jiangsu Higher Education Institutions, Soochow University, 199 Renai Road, Suzhou Industrial Park, Suzhou 215123, People's Republic of China

[§]Department of Chemistry and Biochemistry, Florida State University, Tallahassee, Florida 32306, United States

Supporting Information

ABSTRACT: Two new uranyl vanadates have been prepared from hydrothermal reactions and structurally characterized by single-crystal X-ray diffraction. The structure of $(H_3O)UO_2VO_4$ (**UVO-1**) consists of anionic layers containing UO_2^{2+} pentagonal bipyramids coordinated by edge-sharing VO_5 square pyramids, with the charge balanced by interlaminar H_3O^+ cations. Vanadium in $(UO_2)_3(VO_4)_2(H_2O)_3$ (**UVO-2**) exists as monomeric VO_4 tetrahedra coordinating to UO_2^{2+} pentagonal bipyramids, forming a 3D uranyl(VI) vanadate framework. Similar reactions with the addition of $Ln(NO_3)_3$ (Ln = Nd, Eu) afford the three heterobimetallic lanthanide uranyl vanadate frameworks $Nd(UO_2)_3(VO_4)_3(H_2O)_{11}$ (**NdUVO-1**), $Eu(UO_2)_3(VO_4)_3(H_2O)_{10}$ (**EuUVO-1**), and $Eu_2(UO_2)_{12}(VO_4)_{10}(H_2O)_{24}$ (**EuUVO-2**). In **NdUVO-1** and **EuUVO-1**, Ln^{3+} cations are inserted into the interlayer space of **UVO-1** substituting for H_3O^+ and further bridging adjacent layers into 3D frameworks. Similarly, **EuUVO-2** adopts the same sheet topology as **UVO-2**, with Eu^{3+} ions replacing some of the interlayer uranyl ions in **UVO-2**. Our work has demonstrated that uranyl vanadate extended structures are excellent hosts for further incorporation of trivalent lanthanide/actinide cations and has provided a new way to create new heterobimetallic 4f−5f and 5f−5f compounds.

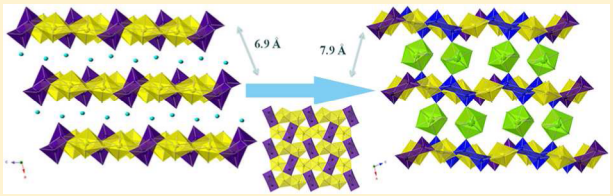

1. INTRODUCTION

There is renewed interest in nuclear power in many technologically advanced nations. Deep geological disposal is a preferred option for the management of nuclear waste in many countries, especially for the vast amounts of used nuclear fuel and other high-level radioactive waste.[1a−c] However, release of high toxicity and long-half-life radionuclides during long-term storage is a primary concern. Furthermore, the migration of hazardous radionuclides creates a significant threat to the environment and public safety.[1c,d] Burns et al. proposed that uranyl compounds formed during corrosion and oxidative alteration of used nuclear fuel can further act as a host to incorporate transuranium elements by charge-balance substitution, which may decrease the mobility of these radionuclides.[2] A new proposed strategy for immobilization of soluble actinide elements utilizing coprecipitation methods at low temperature has been accomplished in recent work; actinyl ions (i.e., NpO_2^+ and UO_2^{2+}) have been successfully incorporated in natural minerals.[3] The sequestration of two key cocontaminants in nuclear waste, ^{237}Np and ^{129}I, has been accomplished by cocrystallization within uranyl(VI) compounds,[4] but little is known about the incorporation of trivalent minor actinides (americium and curium) within uranyl compounds. The separation and sequestration or fissioning of americium is a key component of closed, advanced nuclear fuel cycles. Trivalent lanthanides (primarily Nd^{3+} and Eu^{3+}) have been used as analogues of trivalent transplutonium elements (e.g., Am^{3+} and Cm^{3+}) owing to their nearly identical ionic radii. Therefore, understanding the cocrystallization of trivalent lanthanides with uranyl in heterobimetallic 4f−5f compounds is important for designing new advanced waste forms and for predicting the fate of actinides in the environment. There are only a handful of reports in the literature concerning this family of compounds. Volkringer et al. reported several heterobimetallic uranyl/lanthanide mellitates,[5] which can be used as thermal degradation precursors of mixed 4f−5f or 5f−5f oxide solid solutions. Knope et al. and Liu et al. synthesized heterobimetallic uranyl/lanthanide carboxyphosphonates and germanates, respectively, with interesting photoluminescence sensitization phenomena.[6] A series of ordered and disordered 4f−5f and 5f−5f heterobimetallic diphosphonates were prepared and characterized by Diwu et al.[7]

Recently, the formation of highly insoluble vanadate minerals has been shown to be effective in the remediation of uranium-contaminated groundwater and appears to be superior to phosphate precipitation in many regards.[8] The origin of these improvements lies in the enhanced coordinating abilities of vanadates to uranyl(VI), which is typically found within the UO_2^{2+} moiety. These natural phases control the solubility of

Received: May 20, 2015
Published: August 20, 2015

DOI: 10.1021/acs.inorgchem.5b01141
Inorg. Chem. 2015, 54, 8449−8455

Table 1. Crystallographic Data for $(H_3O)UO_2VO_4$ (UVO-1), $(UO_2)_3(VO_4)_2(H_2O)_3$ (UVO-2), $Nd(UO_2)_3(VO_4)_3(H_2O)_{11}$ (NdUVO-1), $Eu(UO_2)_3(VO_4)_3(H_2O)_{10}$ (EuUVO-1), and $Eu(UO_2)_3(VO_4)_3(H_2O)_{12}$ (EuUVO-2)

	UVO-1	UVO-2	NdUVO-1	EuUVO-1	EuUVO-2
space group	$P2_1/c$	$Pnma$	$P2_1/n$	$P2_1/n$	$P1$
formula wt	403.99	1087.97	1475.15	1466.87	5077.68
a/Å	6.9918(10)	27.108(3)	9.6260(16)	9.537(2)	11.203(2)
b/Å	8.2655(12)	17.7466(17)	10.5128(18)	10.527(2)	13.368(2)
c/Å	10.5062(15)	7.1288(7)	24.793(4)	24.862(5)	15.644(3)
α/deg	90	90	90	90	71.622(5)
β/deg	107.014(4)	90	98.425(4)	98.487(7)	72.296(5)
γ/deg	90	90	90	90	77.051(5)
V/Å^3	580.59(14)	3429.5(6)	2481.9(7)	2468.8(9)	2096.6(6)
Z	4	8	4	4	1
T/K	298	298	298	298	298
λ(Mo Kα)/Å	0.71073	0.71073	0.71073	0.71073	0.71073
ρ/g cm^{-3}	4.622	4.214	3.948	3.903	4.022
μ/cm^{-1}	294.39	293.58	227.48	233.00	257.21
R1 (on F_o^2, $I > 2\sigma(I)$)[a]	0.0197	0.0424	0.0488	0.0584	0.0400
wR2 (on F_o^2, $I > 2\sigma(I)$)[b]	0.0458	0.1193	0.1352	0.1095	0.0874

[a] $R1 = \sum||F_o| - |F_c||/\sum|F_o|$. [b] $wR2 = [\sum w(F_o^2 - F_c^2)^2/\sum w(F_o^2)^2]^{1/2}$.

U(VI) even when phosphate is present and are solubility-limiting products. Owing to the formation of these minerals over a wide range of conditions, a large family of uranyl(VI) vanadate minerals have been identified that include carnotite, curienite, francevillite, tyuyamunite, and metatyuyamunite.[9] Combining variable oxidation states of vanadium and the structural diversity of vanadates, crystalline actinide vanadates could be potential candidates for effectively immobilizing multiple actinide radioisotopes under different environmental conditions,[10] especially for emergent treatment for water systems contaminated with small amounts of uranium and minor actinides.[8] A series of synthetic uranyl vanadates have also been reported and extensively characterized, with the majority adopting 2D anionic layered structures with alkali-metal cations residing in the interlayer space.[11] These aforementioned compounds were synthesized by high-temperature, solid-state reactions. In addition, several organically templated uranyl vanadates have been prepared by traditional hydrothermal methods.[12]

Herein, we report two uranyl(VI) vanadate compounds with different structural topologies that can be used as crystalline hosts for further incorporation of trivalent lanthanides via substitution of components present in the interlayer space, confirmed by X-ray crystallography, UV−vis absorption spectroscopy, energy-dispersive X-ray spectroscopy, and laser-ablation inductively coupled plasma mass spectrometry. Our work is not only helpful in creating new heterobimetallic 4f−5f or 5f−5f compounds but also provides structural information for a further understanding of the incorporation mechanism of trivalent minor actinides into uranyl vanadate minerals in the environment.

2. EXPERIMENTAL SECTION

Caution! *All uranium compounds used in these studies contained depleted uranium; standard precautions were performed for handling radioactive materials, and all studies were conducted in a laboratory dedicated to studies on actinide elements.*

2.1. Reagents. V_2O_3, $Eu(NO_3)_3{\cdot}6H_2O$, $Nd(NO_3)_3{\cdot}6H_2O$, and $UO_2(CH_3COO)_2{\cdot}2H_2O$ were used as received.

2.2. Synthesis of UVO-1 and UVO-2. A 0.1281 g portion of $UO_2(CH_3COO)_2{\cdot}2H_2O$, 0.0236 g of V_2O_3 (U:V molar ratio 1:1), and 2 mL of ultrapure water were loaded into a 10 mL autoclave. The autoclave was then sealed and heated to 200 °C for 3 days under autogenous pressure and cooled to room temperature at a rate of 3.5 °C/h. The product consists of yellow prismatic crystals of (H_3O)-UO_2VO_4 (abbreviated **UVO-1**) as the minor phase and yellow acicular crystals of $(UO_2)_3(VO_4)_2(H_2O)_3$ (abbreviated **UVO-2**) as the major phase, as well as a trace amount of unreacted black V_2O_3.

2.3. Synthesis of NdUVO-1, EuUVO-1, and EuUVO-2. A 0.1281 g portion of $(UO_2)(CH_3COO)_2$, 0.0236 g of V_2O_3, 0.1338 g of $Nd(NO_3)_3{\cdot}6H_2O$ (or 0.1355 g of $Eu(NO_3)_3{\cdot}6H_2O$, Ln:U:V molar ratio 1:1:1), and 2 mL of ultrapure water were loaded into 10 mL autoclaves. The autoclaves were then sealed and heated to 200 °C for 3 days under autogenous pressure and cooled to room temperature at a rate of 3.5 °C/h. Isotypic yellow platelike crystals of Nd-$(UO_2)_3(VO_4)_3(H_2O)_{11}$ (abbreviated **NdUVO-1**) and Eu-$(UO_2)_3(VO_4)_3(H_2O)_{10}$ (abbreviated **EuUVO-1**) were isolated, respectively. $Eu(UO_2)_3(VO_4)_3(H_2O)_{12}$ (abbreviated **EuUVO-2**) was obtained from a reaction extended over 4 days.

2.4. Crystallographic Studies. Crystals were mounted on Cryoloops with Paratone and optically aligned on a Bruker D8-Venture single-crystal X-ray diffractometer equipped with a digital camera. The diffraction data were collected using a Turbo X-ray Source (Mo Kα radiation, λ = 0.71073 Å) adopting the direct-drive rotating anode technique and a CMOS detector at room temperature. The structures were solved by direct methods and refined on F^2 by full-matrix least-squares methods using SHELXTL.[13] For **UVO-1**, all of the non-hydrogen atoms were refined anisotropically and the hydrogen atoms of water molecules were found from the Fourier maps. For **UVO-2**, only atoms (including U, V, and O) present in the 2D uranyl vanadate host layers (see Results and Discussion in the main text) could be refined anisotropically, while the uranium atoms located at the interlayer spaces were partially disordered and could not be refined anisotropically. The disorder treatment can be found in the CIF files in the Supporting Information. For **NdUVO-1** and **EuUVO-1**, only atoms present in the 2D uranyl vanadate host layers could be refined anisotropically, similarly to the case for **UVO-2**. The incorporated lanthanide atoms are partially disordered. For **EuUVO-2**, only uranium atoms could be refined anisotropically, including those in the interlayer spaces. Again, the incorporating lanthanide atoms are partially disordered. The presenting A-level alerts in the checkcif file for **EuUVO-2** are not reasonable, since the maximum shift we observed during refinement was 0.000 Å; however, this could originate from difficulties in refining the coordinating water molecules around disordered Eu^{3+} cations. Attempts to increase the refinement cycles or adjust the site occupancy correspondingly did not solve this issue. Crystallographic data for **UVO-1**, **UVO-2**, **NdUVO-1**, **EuUVO-1**, and **EuUVO-2** are given in Table 1.

DOI: 10.1021/acs.inorgchem.5b01141
Inorg. Chem. 2015, 54, 8449−8455

2.5. Powder X-ray Diffraction. Powder patterns were collected from 5 to 50°, with a step of 0.02° using a Bruker D8 advance X-ray diffractometer with Cu Kα radiation (λ = 1.54056 Å) equipped with a Lynxeye one-dimensional detector.

2.6. UV−Vis Absorption and Photoluminescence Spectroscopy. UV−vis absorption spectra were recorded from single crystals of five phases using a Craic Technologies microspectrophotometer. Crystals were placed on quartz slides, and the data were collected after optimization of the microspectrophotometer. Photoluminescence spectroscopy data were recorded from single crystals of lanthanide-incorporated phases using a Craic Technologies microspectrophotometer. Crystals were placed on quartz slides, and the data were collected after optimization of the microspectrophotometer.

2.7. Laser-Ablation Inductively Coupled Plasma Mass Spectrometry. LA-ICP-MS measurements on single crystals from lanthanide-incorporated phases were conducted using a ThermoFisher Element2 ICP-MS instrument coupled to a UP213 Nd:YAG laser ablation system (New Wave Research).

2.8. Energy-Dispersive X-ray Spectroscopy Analysis. Scanning electron microscopy/energy-dispersive spectroscopy (SEM/EDS) images and data were collected using a FEI Quanta 200FEG instrument. The energy of the electron beam was 30 kV, and the spectrum acquisition time was 100 s.

2.9. IR Spectrum. The infrared spectrum of **UVO-1** was recorded using a single crystal with a Bruker Hyperion instrument in the range of 600−4000 cm^{-1}.

3. RESULTS AND DISCUSSION

3.1. Synthesis. The structure of vanadate oxoanion compounds in hydrothermal systems is greatly controlled by the reaction conditions, such as pH and temperature. Different polymerized vanadate oxoanion species can be obtained by adjusting the solution acidity.[10] In the present work, the reaction of V_2O_3 with uranyl acetate by traditional hydrothermal methods (typically 200 °C and 72 h) results in two distinct uranyl vanadates, the minor phase being yellow prismatic crystals of **UVO-1** and the major phase yellow acicular crystals of **UVO-2**. Trace amounts of unreacted black powder of V_2O_3 are present in the product as well (a microscopic image is shown in Figure S1 in the Supporting Information). Obviously, most of the trivalent vanadium source is oxidized to pentavalent vanadates, possibly by O_2 in the air during the reaction process. A prolonged reaction time (120 h) has no influence on the product. The heterobimetallic 4f−5f compounds **NdUVO-1** and **EuUVO-1** can be obtained under the aforementioned reaction conditions with the addition of 1 equivalent of lanthanide nitrate. Two isotypic compounds can be collected as the pure phases, as demonstrated by the powder X-ray diffraction data (Figure S2 in the Supporting Information). **EuUVO-2** can be isolated as a pure phase by extending the reaction time to 96 h. However, only **NdUVO-1** was obtained from prolonged reaction time (PXRD data are shown in Figure S3 in the Supporting Information). Therefore, it was speculated that the subtle difference in ionic radii between Nd^{3+} and Eu^{3+} greatly affected the reaction process and products.

3.2. Crystal Structures. Single-crystal X-ray diffraction studies revealed that **UVO-1** is isotypic with $(NH_4)_2[(UO_2)_2V_2O_8]$[12b] and crystallizes in the centrosymmetric monoclinic space group $P2_1/c$. The overall structure is based on anionic layers; the crystallographically ordered H_3O^+ distributes in the interlayer space to balance the negative charge of the layers, as shown in Figure 1. The presence of hydronium cation is further confirmed by two weak features at 1680 and 1720 cm^{-1} as well as a broad feature between 3000 and 3500 cm^{-1} in the FTIR micro spectrum measured from a single crystal of **UVO-1** (Figure S4 in the Supporting Information).[14] The layers of **UVO-1** are parallel to the [bc] plane and adopt the carnotite topology,[15] which contain dimers of edge-sharing UO_7 pentagonal bipyramids and dimers of edge-sharing VO_5 square pyramids. Within the VO_5 dimers, the vertices of two adjacent square pyramids point in opposite directions. There is only one crystallographically independent uranium site and one vanadium site in the asymmetric unit. The U−O equatorial bond lengths range from 2.297(3) to 2.376(4) Å, whereas the axial U≡O bonds are 1.806(4) and 1.810(4) Å, respectively. The V−O bond lengths within the square plane range from 1.792(4) to 1.930(4) Å, and the short vertex bond (1.612(4) Å) can be assigned as a vanadyl unit, in comparison to typically observed vanadyl bonds that occur in the range 1.56−1.62 Å.[16] All five equatorial oxygen atoms of uranyl are μ_3-O atoms. The bond valence sums (BVS) calculated for the three oxygen atoms in the asymmetric unit are all close to 2 (O1, 1.92; O3, 1.89; O4, 1.70), indicating their full deprotonation.

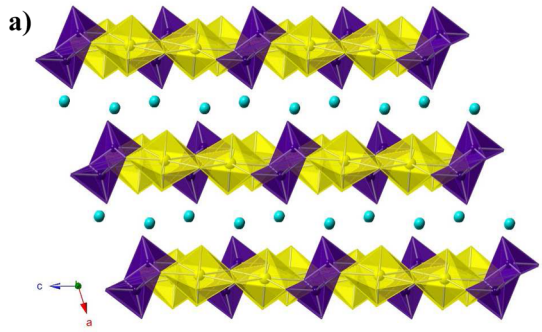

Figure 1. View of the crystal structure of **UVO-1** along the b axis: H_3O^+, light blue; UO_7. yellow; dimers of VO_5, purple.

In contrast, **UVO-2** crystallizes in the orthorhombic system in the space group *Pnma*. Its structure can be best described as a porous 3D framework constructed from uranophane-type layers containing UO_7 pentagonal bipyramids and monomeric VO_4 distorted tetrahedra that are further bridged through additional interlaminar UO_7 polyhedra, as depicted in Figure 2. The asymmetric unit of **UVO-2** consists of four independent U sites and two V sites. The axial and equatorial uranium oxygen bonds range from 1.766(11) to 1.786(12) Å and from 2.316(8)

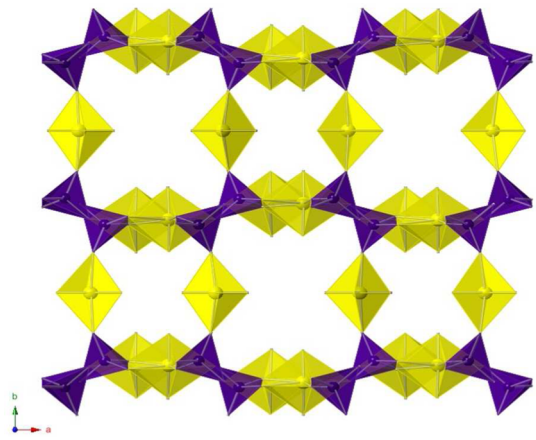

Figure 2. View of the crystal structure of **UVO-2** down the c axis: UO_7, yellow; VO_4, purple. The linkage UO_7 in the interlayer along b axis is distorted with larger crystallographic thermal parameters.

DOI: 10.1021/acs.inorgchem.5b01141
Inorg. Chem. 2015, 54, 8449−8455

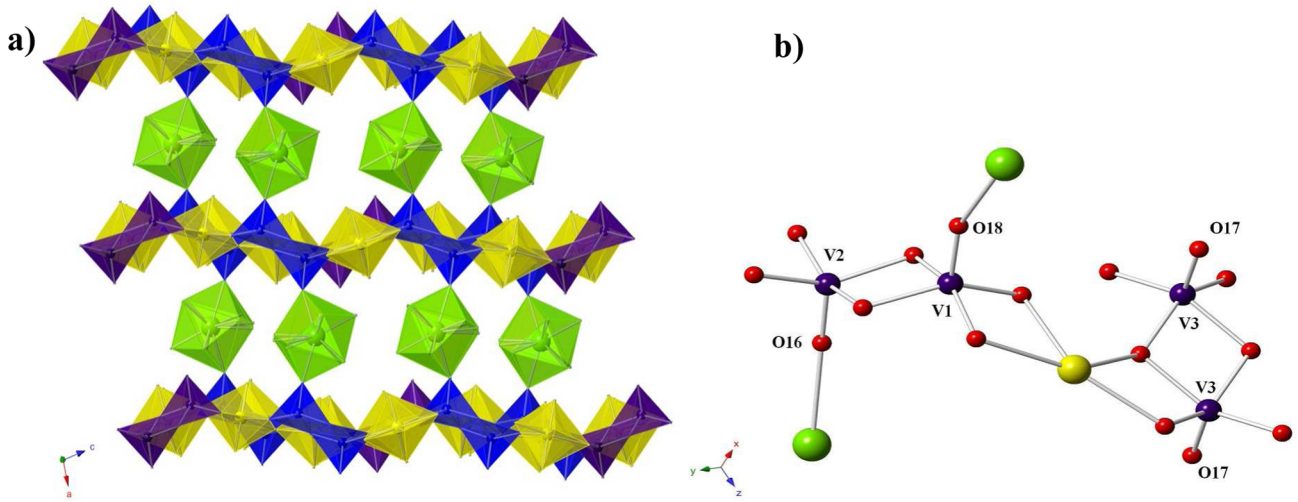

Figure 3. (a) View of the crystal structure of **LnUVO-1** along the *b* axis: UO_7, yellow; LnO_n, green; dimers of VO_5, purple (vanadates without lanthanide coordination) or dark blue (vanadates with lanthanide coordination). (b) Ball-and-stick model for coordinated V═O and terminal V═O in **EuUVO-1**.

Table 2. Summary of the Bond Lengths of V═O in Vanadyl in LnUVO-1

	EuUVO-1			NdUVO-1		
bond	V(1)−O(18)	V(2)−O(16)	V(3)−O(17)	V(4)−O(19)	V(5)−O(18)	V(6)−O(14)
bond length/Å	1.624(15)	1.601(15)	1.578(17)	1.587(13)	1.639(13)	1.601(12)
condition	coordinated to Eu^{3+}	coordinated to Eu^{3+}	terminal	terminal	coordinated to Nd^{3+}	coordinated to Nd^{3+}

to 2.60(3) Å, respectively, while V−O distances within the VO_4 unit range from 1.651(12) to 1.732(8) Å. The uranophane-type layers are built through UO_7 edge-sharing chains (U1 and U2) connected via VO_4 tetrahedra in a corner-sharing mode with UO_7 units in their equatorial planes. The other two uranyl sites (U3 and U4) are coordinated to these VO_4 tetrahedra in the direction perpendicular to the layers (along the *b* axis), thus bridging adjacent layers to afford an open-framework structure with two types of 1D channels extended along the *c* axis. The sizes of the channels are 6.206 × 5.275 Å and 4.461 × 3.244 Å, respectively. Notably, the bridging uranium sites are partially disordered, strongly indicating weaker interlayer interactions between vanadates and bridging uranyl groups in comparison to the corresponding intralayer coordination. Along with the relatively larger crystallographic thermal parameter (U_{eq}) of hydronium oxygen in comparison to others in **UVO-1**, the crystallographic data therefore indicated that both uranyl vanadate compounds could be used as excellent host lattices to incorporate other metal cations in the interlayer space.

The addition of 1 equivalent of $Nd(NO_3)_3{\cdot}6H_2O$ or $Eu(NO_3)_3{\cdot}6H_2O$ to the reaction mixtures (Ln:U:V molar ratio 1:1:1) without a change in any other reaction parameters results in the formation of **NdUVO-1** and **EuUVO-1**. The difference in numbers of coordinated waters binding to the Ln^{3+} center is partially due to the subtle change in ionic radii. The crystal structure of **LnUVO-1** (Ln = Nd, Eu) consists of a 4f−5f heterobimetallic 3D framework built from uranyl vanadate anionic layers linked by interlaminar hydrated Ln^{3+} cations, as shown in Figure 3. **LnUVO-1** crystallizes in the monoclinic space group $P2_1/n$. The asymmetric unit of **EuUVO-1** contains three independent U sites, three V sites, and one Ln site; the uranyl cation also adopts a UO_7 pentagonal-bipyramidal coordination geometry, in which five equatorial oxygen atoms are supplied by a VO_5 square pyramid. The vanadyl units with relatively short V═O bonds provide oxygen atoms to bind to distorted lanthanide cations, constructing a 4f−5f heterobimetallic three-dimensional framework. The U≡O and U−O bond lengths are in the ranges of 1.795(15)−1.850(15) and 2.300(15)−2.384(15) Å, respectively. The significant change in bond length of V═O could be clearly observed in vanadyl units. As shown Figure 3b, bond lengths in V═O coordinating to Eu^{3+} centers (V(1)−O(18) 1.624(15) Å, V(2)−O(16) 1.601(15) Å) are greatly elongated in comparison with the terminal V═O length (V(3)−O(17) 1.578(17) Å), confirming the Lewis basic nature of vanadyl oxygen being similar to that of the bridging uranyl oxygen, formally called cation−cation interactions (CCIs).[17] To the best of our knowledge, this is the first report of the formation of V═O−Ln bonds, further suggesting the potential applications of remediating heavy-metal pollutants using materials containing coordination-available vanadyl oxygen donors.[18] The V═O bond lengths in vanadyl units are summarized in Table 2.

Interestingly, the topology, composition, and arrangement of uranyl vanadate layers in **LnUVO-1** closely resemble those of **UVO-1**, with subtle differences induced by lanthanide insertion (Figure 5a,b). Actually, **LnUVO-1** crystallizes in the space group $P2_1/n$, which is a transformation from the space group of **UVO-1**, $P2_1/c$. In view of the same reaction conditions and the structural similarities between **UVO-1** and **LnUVO-1**, interlayer cations are likely to compete with each other during the formation reactions of **LnUVO-1**: i.e., the hydronium cations in **UVO-1** are substituted by Ln^{3+} cations in the structures. As a result of lanthanide incorporation, the number of independent sites of uranium and vanadium within the layers increases from one to three in **LnUVO-1**, with two-thirds of the VO_5 square pyramids providing vanadyl oxygen to coordinate lanthanide ions. Meanwhile, the presence of lanthanide ions in the interlayer expands the distance between adjacent layers from

DOI: 10.1021/acs.inorgchem.5b01141
Inorg. Chem. 2015, 54, 8449−8455

6.992 Å in **UVO-1** to 7.935 and 7.867 Å in **NdUVO-1** and **EuUVO-1**, respectively. The difference between the last two agrees well with the phenomenon of lanthanide contraction.[12b] The coordination spheres of the incorporating lanthanides are completed by eight additional coordinated water molecules with slight disorder.

For **UVO-2**, which possesses a framework structure, the partially disordered interlayer uranyl ions can also be substituted with prolonged reaction times in the presence of $Eu(NO_3)_3{\cdot}6H_2O$. **EuUVO-2** crystallizes in a triclinic crystal system in the *P*1 space group and is built from uranophane-type vanadate layers bridged by additional uranyl and Eu^{3+} polyhedra, forming a dense three-dimensional framework, as shown in Figure 4. The asymmetric unit of **EuUVO-2** consists

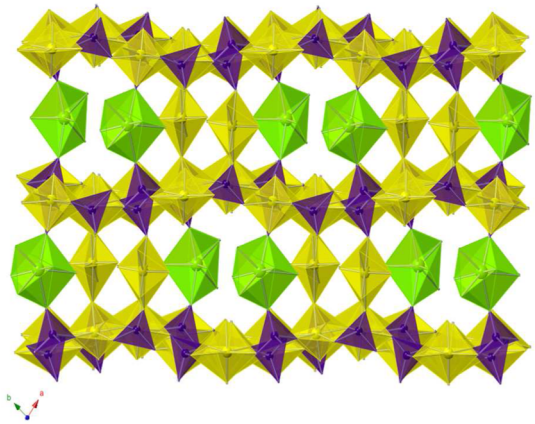

Figure 4. View of crystal structure of **EuUVO-2** down the *c* axis: UO_7, yellow; EuO_n, green; VO_4, purple.

of 12 independent U sites, 10 V sites, and 2 Eu sites. The framework can be divided into two components: a $UO_2VO_4^-$ layer and Eu^{3+}/UO_2^{2+} ions as the linkages. The $UO_2VO_4^-$ layer is constructed from edge-sharing UO_7 pentagonal bipyramids, with three equatorial oxygen atoms provided by the monomeric VO_4 tetrahedron. The linkage UO_2^{2+} ions adopt the coordination geometry of a UO_7 pentagonal bipyramid with O≡U≡O moieties parallel with the $UO_2VO_4^-$ layer; three equatorial oxygen atoms are provided by VO_4 tetrahedra, and the other two are coordinated water. The other linkage Eu^{3+} ions are also bonded by two VO_4 tetrahedra, while Eu^{3+} ions exhibit a distorted-polyhedral coordination geometry with weakly coordinated water. Therefore, a dense three-dimensional framework with low symmetry is constructed. As found in the previous example, the topology of **EuUVO-2** is identical with that of **UVO-2** (Figure 5c,d)) with partial interlayer uranyl ions in **UVO-2** substituted by Eu^{3+} cations, forming a denser 3D framework in comparison to that of **UVO-2**. The distance between adjacent layers in **EuUVO-2** is slightly expanded, owing to the larger ionic radius of Eu^{3+} in comparison to that of uranyl ions. The uranium atoms residing in the interlayer spaces are fully ordered with the UO_7 pentagonal-bipyramidal geometry, while the incorporating Eu^{3+} cations are partially disordered, strongly indicating partial substitution of disordered interlaminar uranium in **UVO-2** with Eu^{3+} in **EuUVO-2**.

3.3. SEM/EDS and LA-ICP-MS Analysis. For further confirmation of the incorporation of lanthanide cations in the uranyl vanadate compounds, SEM/EDS measurements were performed on single crystals. SEM images of four crystals are

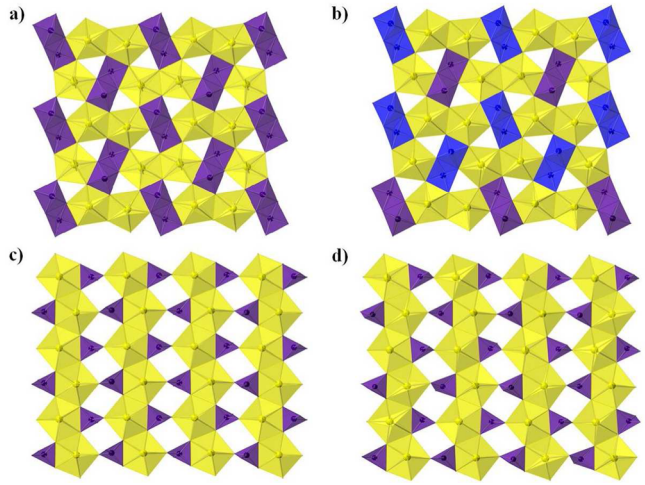

Figure 5. Layer topologies of **UVO-1** (a), **NdUVO-1** (b), **UVO-2** (c), and **EuUVO-2** (d): UO_7, yellow; dimers of VO_5 in **UVO-1** and **NdUVO-1**, purple. Monomeric VO_4 units in **UVO-2** and **EuUVO-2** are also represented in purple. The dark blue in **NdUVO-1** represents vanadates with lanthanide coordination.

shown in Figure 6. Energy-dispersive X-ray spectroscopy of four compounds (Table 3) clearly shows that the atomic ratio is

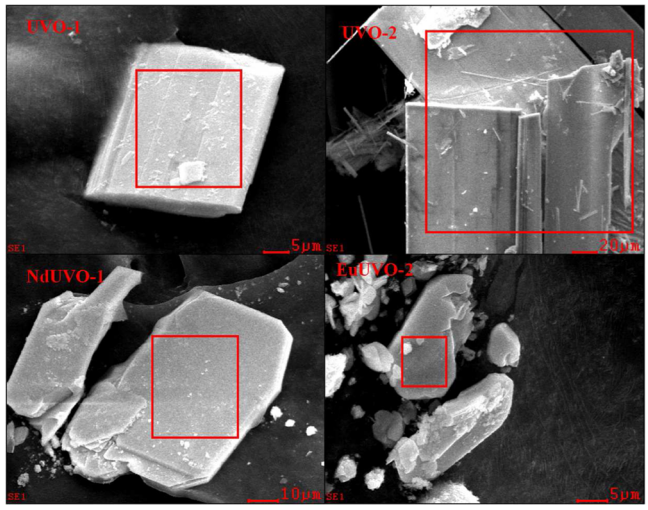

Figure 6. SEM images of **UVO-1**, **UVO-2**, **NdUVO-1**, and **EuUVO-2**.

consistent with the crystallographic results, indicating that lanthanide cations are successfully incorporated into uranyl vanadates. Moreover, crystals of **EuUVO-1**, **EuUVO-1**, and **EuUVO-2** were selected for laser-ablation inductively coupled plasma mass spectrometry to investigate the depth distribution of lanthanides in the crystals of the heterobimetallic compounds. Figure S5 in the Supporting Information demonstrates a typical time-resolved spectrum (i.e., ion signal measured in counts per second (cps) vs time (s)). The background signal measurements show that background count rates are in range of 10−100 cps, while the neodymium signal exhibits enhanced counts when laser ablation was performed on the crystal. The neodymium signal is concomitant with the signal for uranium, indicating that Ln ions are incorporated into the entire crystals of uranyl vanadates instead of being adsorbed on the surface.[19]

DOI: 10.1021/acs.inorgchem.5b01141
Inorg. Chem. 2015, 54, 8449−8455

Table 3. Energy-Dispersive X-ray Spectroscopy Results for Four Selected Compounds

	formula	element/atom % Ln	U	V	O	theor mole ratio
UVO-1	$(H_3O)UO_2VO_4$		9.43	8.25	82.32	U:V = 1:1
UVO-2	$(UO_2)_3(VO_4)_2(H_2O)_3$		10.53	9.61	79.86	U:V = 1.5:1
NdUVO-1	$Nd(UO_2)_3(VO_4)_3(H_2O)_{11}$	3.88	10.01	10.97	75.13	Nd:U:V = 1:3:3
EuUVO-2	$Eu_2(UO_2)_{12}(VO_4)_{10}(H_2O)_{24}$	2.72	11.45	10.89	74.94	Eu:U:V = 1:6:5

3.4. Spectroscopic Properties. Solid-state UV−vis−NIR absorption spectrum of all compounds is shown in Figure 7.

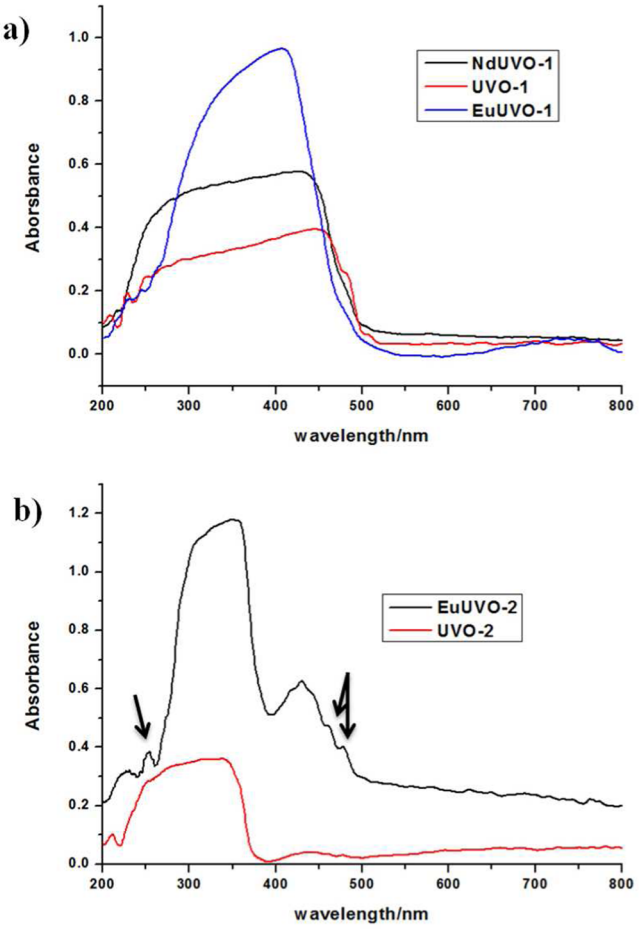

Figure 7. Solid-state UV−vis absorption spectra of **UVO-1**, **NdUVO-1**, and **EuUVO-1** (a) and of **UVO-2** and **EuUVO-2** (b).

The typical charge transfer absorption peaks of equatorial U−O and the axial U≡O are not observed in **NdUVO-1**, **EuUVO-1**, and **UVO-1** due to large charge transfer features from VO_5 units dominating the UV/visible regions,[20] as shown in Figure 7a. Figure 7b provides clear evidence that Eu^{3+} ions are incorporated into uranyl vanadates; arrows indicate the characteristic f−f transitions for Eu^{3+}.[20a] The two peaks from 200 to 500 nm are the vibronic progressions from uranyl and Eu^{3+}.[20] From 200 to 400 nm, there is a superposition of V−O charge transfer and equatorial U−O charge transfer.[21] The features from 400 to 500 nm are the uranyl axial CT bands that are vibronically coupled. Unlike the case for $(UO_2)_2(PPA)(HPPA)_2Sm(H_2O)\cdot 2H_2O$ and $K_4[(UO_2)Eu_2(Ge_2O_7)_2]$,[11] uranyl sensitization for the lanthanide photoluminescence is not observed, likely due to the fluorescence quenching originated from crystallographic disorders of lanthanide cations and nonradiative energy loss through the bound water molecules.

4. CONCLUSION

In conclusion, two new uranyl vanadates have been synthesized, starting with V_2O_3, and trivalent lanthanide cations have been successfully inserted into their layers and frameworks. This intercalation is achieved by combining the stability of the uranyl vanadate layers and the binding of the lanthanide cations by the vanadyl oxo atoms. The structures of **LnUVO-1**, featuring the first V═O−Ln bond reported in a solid-state structure, further suggest the potential applications of remediating heavy-metal pollutants using materials containing coordination-available vanadyl oxygen donors. What we observed in this system are real crystal lattice sites possessed by a chemically robust uranyl vanadate extended structure for effective immobilization of trivalent lanthanides and actinides, which may lead to extra stabilization of minor actinides provided by lattice energy. Our work not only is helpful in creating new heterobimetallic 4f−5f or 5f−5f compounds but also provides structural information for further simultaneous immobilization of trivalent minor actinides with uranyl compounds using vanadate sources as well as further incorporation of trivalent minor actinides into uranyl vanadate minerals in the environment.

■ ASSOCIATED CONTENT

Supporting Information

The Supporting Information is available free of charge on the ACS Publications website at DOI: 10.1021/acs.inorgchem.5b01141.

Powder X-ray diffraction patterns, infrared spectrum, and laser-ablation inductively coupled plasma spectra (PDF)
X-ray crystallographic files for **UVO-1**, **UVO-2**, **NdUVO-1**, **EuUVO-1**, and **EuUVO-2** (CIF)

■ AUTHOR INFORMATION

Corresponding Author

*E-mail for S.W.: shuaowang@suda.edu.cn.

Notes

The authors declare no competing financial interest.

■ ACKNOWLEDGMENTS

This work was supported by the National Natural Foundation of China (91326112, 21422704, 21471107), the Science Foundation of Jiangsu Province (BK20140007), a Project Funded by the Priority Academic Program Development of Jiangsu Higher Education Institutions (PAPD), and "Young Thousand Talented Program" in China. Support for TEA-S was provided by the Chemical Sciences, Geosciences, and Biosciences Division, Office of Basic Energy Sciences, Office of Science, Heavy Elements Chemistry Program, U.S. Department of Energy, under Grant DE-FG02-13ER16414.

DOI: 10.1021/acs.inorgchem.5b01141
Inorg. Chem. 2015, 54, 8449−8455

REFERENCES

(1) (a) Grambow, B. *Elements* **2006**, *2*, 357. (b) Bruno, J.; Ewing, R. C. *Elements* **2006**, *2*, 343. (c) Baker, R. J. *Coord. Chem. Rev.* **2014**, *266-267*, 123. (c) Ewing, R. C. *Nat. Mater.* **2015**, *14*, 252. (d) Maher, K.; Bargar, J. R.; Brown, G. E., Jr. *Inorg. Chem.* **2013**, *52*, 3510.

(2) Burns, P. C.; Ewing, R. C.; Miller, M. L. *J. Nucl. Mater.* **1997**, *245*, 1.

(3) Balboni, E.; Morrison, J. M.; Wang, Z.; Engelhard, M. H.; Burns, P. C. *Geochim. Cosmochim. Acta* **2015**, *151*, 133.

(4) (a) Meredith, N. A.; Polinski, M. J.; Lin, J.; Simonetti, A.; Albrecht-Schmitt, T. E. *Inorg. Chem.* **2012**, *51*, 10480. (b) Wu, S.; Chen, F.; Simonetti, A.; Albrecht-Schmitt, T. E. *Environ. Sci. Technol.* **2010**, *44*, 3192.

(5) (a) Mihalcea, I.; Volkringer, C.; Henry, N.; Loiseau, T. *Inorg. Chem.* **2012**, *51*, 9610. (b) Volkringer, C.; Henry, N.; Grandjean, S.; Loiseau, T. *J. Am. Chem. Soc.* **2012**, *134*, 1275.

(6) (a) Knope, K. E.; de Lill, D. T.; Rowland, C. E.; Cantos, P. M.; de Bettencourt-Dias, A.; Cahill, C. L. *Inorg. Chem.* **2012**, *51*, 201. (b) Liu, S.-P.; Chen, M.-L.; Chang, B.-C.; Lii, K.-H. *Inorg. Chem.* **2013**, *52*, 3990.

(7) Diwu, J.; Wang, S.; Good, J. J.; DiStefano, V. H.; Albrecht-Schmitt, T. E. *Inorg. Chem.* **2011**, *50*, 4842.

(8) (a) Tokunaga, T. K.; Kim, Y.; Wan, J. *Environ. Sci. Technol.* **2009**, *43*, 5467. (b) Tokunaga, T. K.; Kim, Y.; Wan, J.; Yang, L. *Environ. Sci. Technol.* **2012**, *46*, 7471.

(9) (a) Stern, T. W.; Stieff, L. R.; Girhard, M. N.; Meyrowitz, R. *Am. Mineral.* **1956**, *41*, 187. (b) Baran, E. J.; Botto, I. L. *Monatsh. Chem.* **1976**, *107*, 633. (c) Botto, I. L.; Baran, E. J. *Z. Anorg. Allg. Chem.* **1976**, *426*, 321. (d) Frost, R. L.; Cejka, J.; Weier, M. L.; Martens, W.; Henry, D. A. *Vib. Spectrosc.* **2005**, *39*, 131.

(10) Chirayil, T.; Zavalij, P. Y.; Whittingham, M. S. *Chem. Mater.* **1998**, *10*, 2629.

(11) (a) Dion, C.; Obbade, S.; Raekelboom, E.; Abraham, F.; Saadi, M. *J. Solid State Chem.* **2000**, *155*, 342. (b) Obbade, S.; Dion, C.; Duvieubourg, L.; Saadi, M.; Abraham, F. *J. Solid State Chem.* **2003**, *173*, 1. (c) Obbade, S.; Dion, C.; Rivenet, M.; Saadi, M.; Abraham, F. *J. Solid State Chem.* **2004**, *177*, 2058. (d) Obbade, S.; Duvieubourg, L.; Dion, C.; Abraham, F. *J. Solid State Chem.* **2007**, *180*, 866. (e) Obbade, S.; Renard, C.; Abraham, F. *J. Solid State Chem.* **2009**, *182*, 413.

(12) (a) Jouffret, L.; Shao, Z. M.; Rivenet, M.; Abraham, F. *J. Solid State Chem.* **2010**, *183*, 2290. (b) Rivenet, M.; Vigier, N.; Roussel, P.; Abraham, F. *J. Solid State Chem.* **2007**, *180*, 713.

(13) Sheldrick, G. M. *SHELXTL*; Siemens Analytical X-ray Instruments: Madison, WI, 2001.

(14) Stoyanov, E. S.; Kim, K. C.; Reed, C. A. *J. Am. Chem. Soc.* **2006**, *128*, 1948.

(15) Burns, P. C. *Can. Mineral.* **2005**, *43*, 1839.

(16) Schindler, M.; Hawthorne, F. C.; Baur, W. H. *Chem. Mater.* **2000**, *12*, 1248.

(17) Sullens, T. A.; Jensen, R. A.; Shvareva, T. Y.; Albrecht-Schmitt, T. E. *J. Am. Chem. Soc.* **2004**, *126*, 2676.

(18) (a) Sarina, S.; Bo, A.; Liu, D.; Liu, H.; Yang, D.; Zhou, C.; Maes, N.; Komarneni, S.; Zhu, H. *Chem. Mater.* **2014**, *26*, 4788. (b) Banerjee, C.; Dudwadkar, N.; Tripathi, S. C.; Gandhi, P. M.; Grover, V.; Kaushik, C. P.; Tyagi, A. K. *J. Hazard. Mater.* **2014**, *280*, 63.

(19) Wang, S.; Diwu, J.; Simonetti, A.; Booth, C. H.; Albrecht-Schmitt, T. E. *Environ. Sci. Technol.* **2011**, *45*, 9457.

(20) (a) Binnemans, K.; Gorllerwalrand, C. *Chem. Phys. Lett.* **1995**, *235*, 163. (b) Denning, R. G. *J. Phys. Chem. A* **2007**, *111*, 4125.

(21) (a) Eaton, T.; Lin, J.; Cross, J. N.; Stritzinger, J. T.; Albrecht-Schmitt, T. E. *Chem. Commun.* **2014**, *50*, 3668. (b) Lin, J.; Diefenbach, K.; Fu, J.; Cross, J. N.; Clark, R. J.; Albrecht-Schmitt, T. E. *Inorg. Chem.* **2014**, *53*, 9058.

DOI: 10.1021/acs.inorgchem.5b01141
Inorg. Chem. 2015, 54, 8449−8455